IOP Publishing New J. Phys. 25 (2023) 123023 https://doi.org/10.1088/1367-2630/ad1140

New Journal of Physics
The open access journal at the forefront of physics

Deutsche Physikalische Gesellschaft DPG
IOP Institute of Physics

Published in partnership with: Deutsche Physikalische Gesellschaft and the Institute of Physics

OPEN ACCESS

RECEIVED
14 August 2023

REVISED
8 November 2023

ACCEPTED FOR PUBLICATION
30 November 2023

PUBLISHED
11 December 2023

PAPER

Topological phase in a nonreciprocal Kitaev chain

Yu Yan[1], Wen-Xue Cui[2], Shutian Liu[1,*], Ji Cao[2,*], Shou Zhang[2] and Hong-Fu Wang[2,*]

[1] School of Physics, Harbin Institute of Technology, Harbin, Heilongjiang 150001, People's Republic of China
[2] Department of Physics, College of Science, Yanbian University, Yanji, Jilin 133002, People's Republic of China
* Authors to whom any correspondence should be addressed.

E-mail: stliu@hit.edu.cn, caoji@ybu.edu.cn and hfwang@ybu.edu.cn

Keywords: topological phase, nonreciprocity, Kitaev chain

Abstract

We systematically investigate the nonreciprocal Kitaev chain, where the nonreciprocity arises from the hopping amplitude and pairing strength. By studying the Hamiltonians under three different bases, we reveal that the nonreciprocal hopping amplitude cannot induce a topological phase transition, but can result in the complex energy spectrum and non-Hermitian skin effect. Moreover, the Majorana zero energy edge modes, which are robust against the nonreciprocal hopping amplitude, exist stably in the topologically nontrivial phase. On the other hand, the nonreciprocal pairing strength can trigger a topological phase transition, which is associated with the pseudo-Hermitian symmetry breaking. More interestingly, we observe that the exceptional points independent of the topological phase can be determined by the dispersion relation, and there is no non-Hermitian skin effect in the system. Furthermore, we calculate the topological invariant to demonstrate the validity of the bulk-edge correspondence in the pseudo-Hermitian symmetry-unbroken region. Our investigation provides a path to explore the fundamental physics pertaining to the interplay between nonreciprocity and topology in the non-Hermitian topological superconductors.

1. Introduction

The simplest model of topological superconductors, introduced first by Kitaev [1], is the mean Bogoliubov–de Gennes (BdG) Hamiltonian of spinless fermions in one dimension (1D). In general, spinless fermions are regarded as a toy model for the more complicated spinful case or fermions spin-polarized fully. Topological superconductors, as a nascent state of matter, have significantly captured the interest of researchers in recent years, notably the Kitaev model. The open chain of this model exhibits two physical regimes, topologically trivial and nontrivial phases, which are determined by the absence and presence of Majorana zero energy modes localized at the edges of chain [2–4]. In addition to the original Kitaev model, alternative versions such as bosonic and ladder models have been proposed [5–8], revealing a range of intriguing physical phenomena. On the other hand, the robustness of the Majorana zero energy modes against disorders and perturbations theoretically makes them crucial in the topological quantum fault-tolerant calculations [9–11]. Moreover, the experimental observation of Majorana zero energy modes in some materials [12–18] has further highlighted the potential for practical applications in topological superconductors.

Non-Hermitian open systems [19, 20], which interact with their environment, are typically considered to be a subsystem of an infinite Hermitian system. Their complex eigenvalues lead to a number of fascinating physical phenomena. Unlike their Hermitian counterparts, these open quantum systems are described by non-Hermitian Hamiltonians, which allow for the exploration of unconventional physics in various fields, including optics, acoustics, and cold atoms. The introduction of gain and loss to non-Hermitian systems [21–26] have been extensively investigated, revealing a wealth of intriguing and unexpected results, such as purely real energy spectrum. Non-Hermitian system with the nonreciprocity was first proposed to study the localization transition [27], and since then, various novel topological properties of such systems have been investigated, such as new topological invariants [28–31], edge states [32–35], exceptional

point [36–41], anomalous topological transition [42–48], and non-Hermitian skin effect [49–55]. One of the most significant properties of non-Hermitian systems is the breaking of bulk-edge correspondence, where the bulk topological invariants of the energy spectrum cannot predict the occurrence of edge states in the band gap. This observation has led to the development of non-Bloch band theory, which aims to describe the non-Bloch bulk-edge correspondence relation [56–60].

Due to dual focus on topological superconductors and non-Hermiticity, there has been significant interest in the non-Hermitian Kitaev models [61–66]. The non-Hermiticity of these models can be fully added to the on-site chemical potential in various ways. Zeng *et al* [64] demonstrated that topologically nontrivial phase region becomes narrower when imaginary potentials are added to all lattice sites. However, the Majorana bound states always exist stably when imaginary potentials are only added to the two ends of the chain. In the case of the non-Hermitian Kitaev model with $\mathcal{PT}$-symmetry, a topologically trivial region and two different nontrivial regions are observed [65]. It is also clarified that $\mathcal{PT}$-symmetry breaking is independent of the topological phase [66]. The nonreciprocal Kitaev chain with nonreciprocal hopping amplitude and pairing strength is an interesting system to study its non-Hermitian and nonreciprocal nature. It is expected that the nonreciprocal hopping amplitude and pairing strength will break the symmetries and lead to a topological phase transition. However, the topological properties are not yet fully understood. One possible proposal to studying the topological properties of a Kitaev chain with imbalanced pairing terms [67] is to use the extended Zak phase, which has been defined in terms of the biorthonormal inner product under the influence of the conditional imbalance. Another proposal is to investigate the defective Majorana zero modes and number-anomalous bulk-boundary correspondence in the the dimerized non-Hermitian Kitaev chain [68]. Overall, the nonreciprocal Kitaev chain with nonreciprocal hopping amplitude and pairing strength is promising system for studying the interplay between nonreciprocity and topology. Further research is necessary to fully comprehend the topological properties of the system and its potential applications in topological quantum computing.

In this paper, we focus on unraveling the effects of nonreciprocal hopping amplitude and pairing strength on the Kitaev chain. We find that the energy spectrum of the system become complex upon the introduction of nonreciprocal hopping amplitude, which is also readily obtained from the dispersion relation. Remarkably, we highlight the presence of a non-Hermitian skin effect and absence of any topological phase transition as the nonreciprocal hopping amplitude increases. Moreover, the Majorana zero energy edge modes, which are robust to the nonreciprocal hopping amplitude, exist stably in the topologically nontrivial region. On the other hand, within the nonreciprocal Kitaev chain featuring exclusively nonreciprocal pairing strength, we observe that the system undergoes a topological phase transition, accompanied by the breakdown of the pseudo-Hermitian symmetry. Notably, the breakdown of the pseudo-Hermitian symmetry is independent of the topological phase, where corresponding exceptional points can be deduced from the dispersion relation. Furthermore, it is essential to highlight that the non-Hermitian skin effect is invalid due to the inherent equilibrium within the overall system under the Majorana basis. In this framework, the next-nearest-neighbor hopping amplitudes between two distinct types of Majorana fermions are opposite, resulting in the absence of any generated magnetic flux. In the meanwhile, we observe that the Majorana zero energy edge modes also exist in an open chain, and the corresponding topological invariant is calculated in the pseudo-Hermitian symmetry-unbroken region, demonstrating the bulk-edge correspondence relationship in such a nonreciprocal Kitaev chain.

The paper is organized as follows: in section 2, we derive the Hamiltonian of the nonreciprocal Kitaev chain with nonreciprocal hopping amplitude and pairing strength, obtain the dispersion relation of the energy spectrum, analyze the symmetries of the system, and illustrate the schematic diagram in the Majorana basis. In section 3, we first briefly review the concepts of the inverse participation ratio (IPR) and fractal dimension, and then display the effects of the nonreciprocal nearest-neighbor hopping amplitude and pairing strength on the nonreciprocal Kitaev chain, respectively. In section 4, we calculate the topological invariant in the pseudo-Hermitian symmetry-unbroken region, i.e. the winding number. Finally, a conclusion is given in section 5.

2. System and Hamiltonian

We explore a 1D p-wave superconducting Kitaev chain with nonreciprocal hopping amplitude and pairing strength, as illustrated in figure 1(a). The fermionic Hamiltonian is given by ($\hbar = 1$)

$$H = \sum_{j=1}^{N-1} \left(t_1 a_{j+1}^{\dagger} a_j + t_2 a_j^{\dagger} a_{j+1} + \Delta_1 a_{j+1}^{\dagger} a_j^{\dagger} + \Delta_2 a_j a_{j+1} \right) + \sum_{j=1}^{N} \mu a_j^{\dagger} a_j, \tag{1}$$

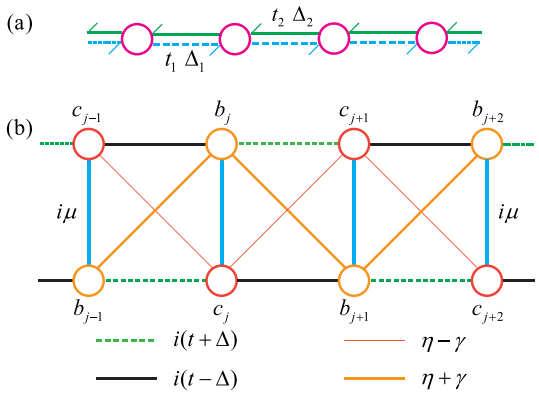

Figure 1. Schematic diagram of the 1D p-wave superconductor Kitaev chain with nonreciprocal hopping amplitude and pairing strength. (a) In real space. The pink circles denote spinless fermion with the chemical potential μ. The blue dashed (green solid) arrows indicate the rightward (leftward) nearest-neighbor interactions including hopping amplitude t_1 (t_2) and p-wave superconducting pairing strength Δ_1 (Δ_2), respectively. (b) In the Majorana basis. The orange and red circles represent two different kinds of the Majorana fermions b and c, respectively.

where $a_j^\dagger$ (a_j) is the creation (annihilation) operator of the spinless fermion at the jth lattice site, $t_{1,2}$ ($\Delta_{1,2}$) describes the nearest-neighbor nonreciprocal hopping amplitude (p-wave superconducting pairing strength), μ is the on-site chemical potential, and N is the size of the system. We define $a_{N+1}=0$ ($a_{N+1}=a_1$) for an open (a closed) chain. For simplicity, we set $t_1=t+\eta$, $t_2=t-\eta$, $\Delta_1=\Delta+\gamma$, and $\Delta_2=\Delta-\gamma$, respectively. t (Δ) describes the constant nearest-neighbor hopping amplitude (pairing strength) and is set as the unit of energy. η and γ denote the nonreciprocity of the nearest-neighbor hopping amplitude and p-wave superconducting pairing strength. Obviously, the non-Hermiticity of the system arises from both the hopping amplitude and pairing strength rather than the on-site chemical potential. Without loss of generality, the parameters involved are real numbers. The Hamiltonian in equation (1) can be physically implemented via the optomechanical system [69, 70].

Due to the particle–hole symmetry (PHS), the Hamiltonian (1) can be diagonalized by the BdG transformation

$$\psi_n^\dagger=\sum_{j=1}^{N}\left[u_{n,j}a_j^\dagger+v_{n,j}a_j\right], \tag{2}$$

where $\psi_n^\dagger$ denotes the BdG operator, n ($n=1,2,\cdots,N$) is the index of energy level, and two complex coefficients $u_{n,j}$ and $v_{n,j}$ are the components of wave functions. The BdG Hamiltonian in the Nambu space can be written as

$$H=\frac{1}{2}\sum_{n=1}^{L}\psi_n^\dagger H_{\mathrm{BdG}}\psi_n, \tag{3}$$

where the matrix form of the core Hamiltonian H_{BdG} is given by

$$H_{\mathrm{BdG}}=\begin{pmatrix} A & B & 0 & \cdots & \cdots & \cdots & C_1\\ B_1 & A & B & 0 & \cdots & \cdots & 0\\ 0 & B_1 & A & B & 0 & \cdots & 0\\ \vdots & \ddots & \ddots & \ddots & \ddots & \ddots & \vdots\\ 0 & \cdots & 0 & B_1 & A & B & 0\\ 0 & \cdots & \cdots & 0 & B_1 & A & B\\ C & \cdots & \cdots & \cdots & 0 & B_1 & A \end{pmatrix}, \tag{4}$$

with

$$A=\begin{pmatrix}\mu & 0\\ 0 & -\mu\end{pmatrix}, B=\begin{pmatrix}t_2 & -\Delta_1\\ \Delta_2 & -t_1\end{pmatrix}, B_1=\begin{pmatrix}t_1 & \Delta_1\\ -\Delta_2 & -t_2\end{pmatrix}, \tag{5}$$

and for the system under periodic boundary condition (PBC),

$$C=B,\ \ C_1=B_1, \tag{6}$$

while for the system under open boundary condition (OBC),

$$C = C_1 = \begin{pmatrix} 0 & 0 \\ 0 & 0 \end{pmatrix}. \tag{7}$$

Obviously, H_{BdG} is a $2N \times 2N$ matrix. Besides, we introduce the wave function in the nth energy band index

$$|\phi_n\rangle = \left(u_{n,1}, v_{n,1}, u_{n,2}, v_{n,2}, \ldots, u_{n,N}, v_{n,N}\right)^{\mathrm{T}}, \tag{8}$$

to derive the bulk BdG equations

$$\begin{aligned} \Delta_1\left(v_{j-1} - v_{j+1}\right) + t_1 u_{j-1} + t_2 u_{j+1} + \mu u_j &= E_n u_j, \\ -\Delta_2\left(u_{j-1} - u_{j+1}\right) - t_1 v_{j+1} - t_2 v_{j-1} - \mu v_j &= E_n v_j. \end{aligned} \tag{9}$$

Therefore, the energy spectrum and state distribution at the jth lattice site of the system can be directly obtained through the above equations.

Furthermore, we derive the Hamiltonian in the momentum space to obtain the dispersion relation of the energy spectrum and boundary conditions of the topological phase transition. By performing the Fourier transformations

$$\begin{aligned} a_j &= \frac{1}{\sqrt{N}} a_k \mathrm{e}^{\mathrm{i}kj}, \quad a_j = \frac{1}{\sqrt{N}} a_{-k} \mathrm{e}^{-\mathrm{i}kj}, \\ a_j^{\dagger} &= \frac{1}{\sqrt{N}} a_k^{\dagger} \mathrm{e}^{-\mathrm{i}kj}, \quad a_j^{\dagger} = \frac{1}{\sqrt{N}} a_{-k}^{\dagger} \mathrm{e}^{\mathrm{i}kj}, \end{aligned} \tag{10}$$

we can acquire the BdG Hamiltonian $H = \frac{1}{2}\Psi_k^{\dagger}\mathcal{H}(k)\Psi_k$, where $\Psi_k = (a_k, a_{-k}^{\dagger})^{\mathrm{T}}$ is the basis in the Nambu space and the core Hamiltonian $\mathcal{H}(k)$ is presented as

$$\mathcal{H}(k) = \begin{pmatrix} \Omega_+ & -2i\Delta_1 \sin k \\ 2i\Delta_2 \sin k & \Omega_- \end{pmatrix}, \tag{11}$$

with $\Omega_{\pm} = \pm\Omega - i(t_1 - t_2)\sin k$ and $\Omega = \mu + (t_1 + t_2)\cos k$. According to the secular equation of the system, the dispersion relation can be expressed as

$$E(k) = \pm\sqrt{(\mu + 2t\cos k)^2 + 4\left(\Delta^2 - \gamma^2\right)\sin^2 k} - 2i\eta \sin k. \tag{12}$$

Now we focus on the phase boundary in the thermodynamic limit, which is determined by the equation $E(k) = 0$. We have $\mu = \pm 2t$ when $k = m\pi$ $(m = 0, 1, \cdots)$, $|\gamma| = \sqrt{\eta^2 + \Delta^2 + \mu^2/4}$ when $k = (1/2 + m)\pi$, and $\mu = 2(-t\cos k \pm \sqrt{\Delta^2 + \eta^2 - \gamma^2}\sin k)$ otherwise. The energy spectrum is complex if $\eta \neq 0$, $\gamma = 0$, and then becomes purely real or imaginary when $\eta = 0$, $\gamma \neq 0$. For the more general case when neither η nor γ is zero, the energy spectrum can exhibit purely real, purely imaginary, zero, and complex values (see appendix for details).

Before discussing reduced model in the Majorana basis, we first focus on the symmetry of the system according to [38, 39, 46]. The Hamiltonian in equation (11) can be written in the compact form

$$\mathcal{H}(k) = h_0\sigma_0 + h_x\sigma_x + h_y\sigma_y + h_z\sigma_z, \tag{13}$$

where σ_0 is the identity matrix and $\sigma_{x,y,z}$ denote the Pauli matrices. The coefficients satisfy $h_0 = -2i\eta\sin k$, $h_x = -2i\gamma\sin k$, $h_y = 2\Delta\sin k$, and $h_z = 2t\cos k + \mu$. The system has the time-reversal symmetry (TRS) defined as a complex conjugation operator $\mathcal{T}\mathcal{H}(k)\mathcal{T}^{-1} = \mathcal{H}(-k)$ and PHS $\mathcal{C}\mathcal{H}^{\mathrm{T}}(k)\mathcal{C}^{-1} = -\mathcal{H}(-k)$ with $\mathcal{C} = \sigma_x$. Also, the system naturally possesses the chiral symmetry (CS) $\mathcal{S} = \mathcal{T}\mathcal{C}$. Thus, the topological invariant of the system is characterized by Z index.

We further introduce the Majorana basis to rewrite equation (1). In general, the Dirac fermion operator a_j can be written as the combination of two Majorana fermion operators b_j and c_j,

$$a_j = \frac{1}{2}\left(b_j + ic_j\right), \quad a_j^{\dagger} = \frac{1}{2}\left(b_j - ic_j\right), \tag{14}$$

which is true since the antiparticle of the Majorana fermion is itself. The Majorana fermion satisfies the anticommutation relation $\{\alpha_j, \beta_{j'}\} = 2\delta_{\alpha,\beta}\delta_{j,j'}$ $(\alpha, \beta = b/c)$. Then the Hamiltonian in equation (1) is rewritten as

$$H_{\mathrm{M}} = \frac{1}{2}\left[(\eta + \gamma)\, b_{j+1}b_j + (\eta - \gamma)\, c_{j+1}c_j + i(t - \Delta)\, b_{j+1}c_j + i(t + \Delta)\, b_j c_{j+1} + \mu\left(1 + ib_j c_j\right)\right]. \tag{15}$$

The schematic diagram according to equation (15) is shown in figure 1(b). The nonreciprocal Kitaev chain can be considered as two coupled Su–Schrieffer–Heeger (SSH) chains [71, 72] with the next-nearest-neighbor hopping amplitude. The system features two different types of Majorana fermions b and c, represented by orange and red circles, respectively. The next-nearest-neighbor hopping amplitudes between Majorana fermions of the same type (orange for b, red for c) are denoted by $\eta+\gamma$ (for b) and $\eta-\gamma$ (for c), which are shown as solid orange and red lines, respectively. The alternating nearest-neighbor hopping amplitudes between different types of Majorana fermions, i.e. between b and c for different sites, are shown as black solid and green dashed lines, corresponding to $i(t-\Delta)$ and $i(t+\Delta)$, respectively. Finally, the next-nearest-neighbor hopping amplitudes, denoted by $i\mu$, are shown as solid blue lines for the same site.

3. Results and discussions

3.1. The IPR and fractal dimension

Before discussing the topological properties of the system under different regimes, we briefly review the concepts of the IPR and fractal dimension of the wave function [73–75]. It is well known that the IPR and fractal dimension are usually used to quantify the localization–delocalization transition. Here we utilize these diagnostic tools to intuitively distinguish whether the non-Hermitian skin effect exists or not. For any given wave function of the system, the IPR of the nth eigenstate is defined as

$$\mathrm{IPR}_n=\frac{\sum_j^N\left(u_{n,j}^4+v_{n,j}^4\right)}{\left[\sum_j^N\left(u_{n,j}^2+v_{n,j}^2\right)\right]^2}, \tag{16}$$

which measures the reciprocal of the number of sites occupied by particles, rather than the number of sites occupied by particles. For a localized state, the IPR approaches 1 since only finite number of sites are occupied, whereas it goes to 0 for an extended state in thermodynamic limit. Another tool, the fractal dimension of the wave function, is described as

$$\Gamma=-\lim_{N\to\infty}\frac{\log(\mathrm{IPR})}{\log N}. \tag{17}$$

Contrary to the IPR, the fractal dimension Γ approaches 1 for an extended state, while Γ goes to 0 for a localized state in thermodynamic limit.

3.2. The nonreciprocal Kitaev model with only nonreciprocal hopping amplitude

We numerically solve equation (4) to obtain the topological properties of the nonreciprocal Kitaev chain when $\eta\neq0$ and $\gamma=0$, as shown in figure 2. Firstly, we present the real and imaginary parts of the energy spectrum, as well as the fractal dimension Γ as a function of μ when $\eta=1$ in figures 2(a) and (b). We find that the present system supports topologically nontrivial and trivial phases, separated by two topological phase transition points at $\mu=\pm2$, as shown in figure 2(a). Notably, except for $\mu=0$ and two topological phase transition points, we observe that both the edge and bulk states are localized due to the fractal dimension $\Gamma\to0$, which reflects the non-Hermitian skin effect unique to the non-Hermitian system. Moreover, the imaginary part of the energy spectrum always exists throughout the entire interval of μ, as depicted in figure 2(b). In figures 2(c) and (d), we illustrate the real and imaginary parts of the energy spectrum, as well as the fractal dimension Γ as a function of η in the topologically nontrivial region ($\mu=0.5$). It is indicated that the degenerate Majorana zero energy modes persist across the entire range of η, as shown in figure 2(c), implying that the nonreciprocal hopping amplitude η cannot induce a topological phase transition. Furthermore, as illustrated in figure 2(d), the imaginary part of the energy spectrum appears immediately as long as $\eta\neq0$, which aligns with the previous analytic discussions on equation (12).

To further demonstrate the fate of Majorana zero energy modes and topological phase transition, we present the minimum absolute eigenvalues of the energy spectrum under OBC and the energy band gap under PBC in the μ–η plane, as shown in figures 2(e) and (f), respectively. We observe that the degenerate Majorana zero energy edge modes always appear (disappear) in the topologically nontrivial (trivial) region between the two white dashed lines, independent of the nonreciprocal hopping amplitude η, as shown in figure 2(e). This provides further evidence that η cannot induce a topological phase transition. In figure 2(f), one can see that there is an opening–closing–reopening process of the energy band gap marked by the two white dashed lines at $\mu=\pm2$ for all η, which indicates that the system undergoes a topological phase transition from the topologically trivial phase to nontrivial phase, and then back to the trivial phase. In other

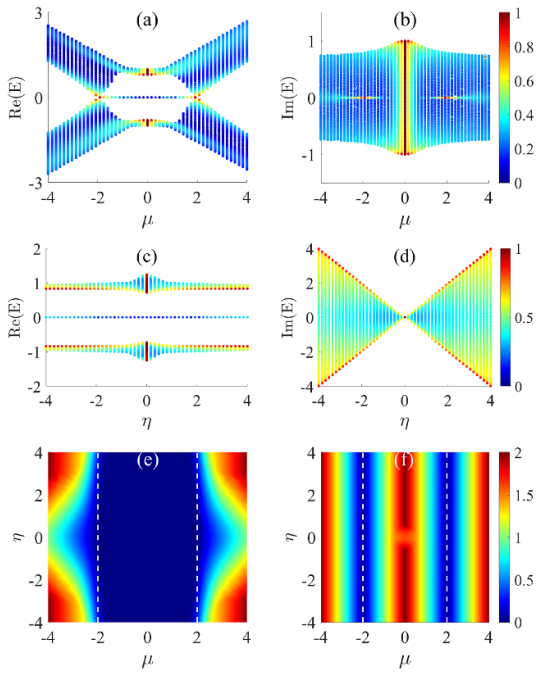

Figure 2. (a) The real and (b) imaginary parts of the energy spectrum, as well as the fractal dimension Γ of the system as a function of μ when $\eta = 1$ under OBC. (c) The real and (d) imaginary parts of the energy spectrum, as well as the fractal dimension Γ of the system as a function of η in the topologically nontrivial region ($\mu = 0.5$). (e) The minimum values of $|E|$ under OBC and (f) the energy band gap under PBC in the μ–η plane. The white dashed lines represent the phase boundary. The rest parameters are set as $t = 1$, $\Delta = 0.8$, $\gamma = 0$, and $N = 100$.

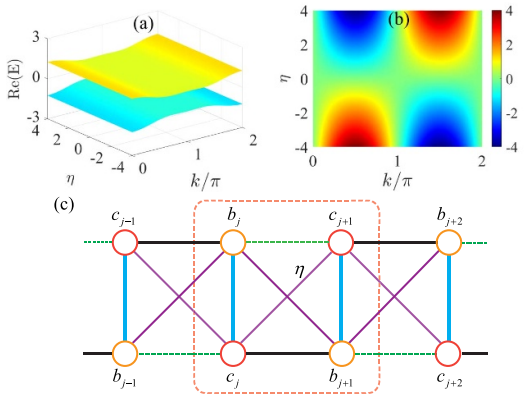

Figure 3. (a) The real part of the energy spectrum as a function of k and η when $\gamma = 0$ and $\mu = 0.5$ in the momentum space. (b) The imaginary part of the energy spectrum in the k–η plane. (c) The schematic diagram in the Majorana basis. The next-nearest-neighbor hopping amplitudes between the same types of Majorana fermions b or c both are η tagged as purple solid lines. The red dotted box represents a unit cell.

words, the nonreciprocal hopping amplitude η does not alter the topological phase or phase transition points of the system.

To gain a deeper understanding of the physical mechanisms, we also analyze the real and imaginary parts of the energy spectrum in the momentum space, as depicted in figures 3(a) and (b). We observe that the energy spectrum is purely real when either $\eta = 0$ or $k = m\pi$, and complex otherwise, which is in agreement with equation (12). Furthermore, the schematic diagram of the nonreciprocal Kitaev chain in the Majorana basis is exhibited in figure 3(c), which can be regarded as two SSH lattice chains coupled to each other with the next-nearest-neighbor hopping amplitude η. This coupling makes the whole system unbalanced, resulting in the non-zero magnetic flux, which leads to the appearance of the non-Hermitian skin effect and complex energy spectrum.

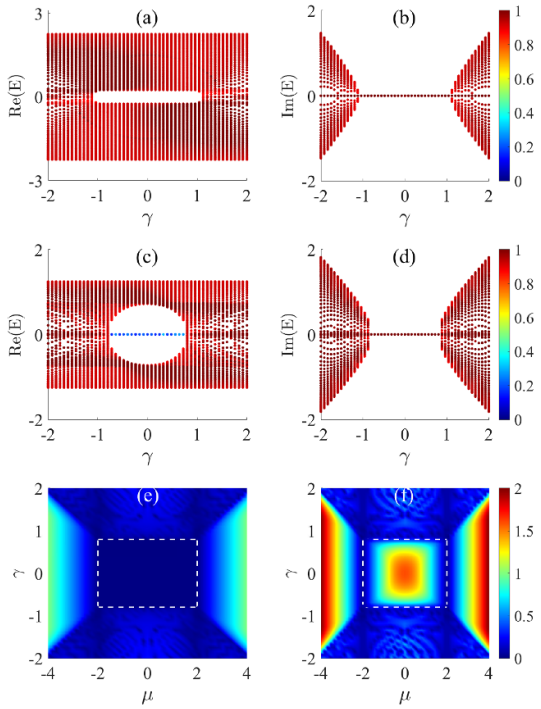

Figure 4. (a) The real and (b) imaginary parts of the energy spectrum, as well as the fractal dimension as a function of γ in topologically trivial region ($\mu = 2.5$). (c) The real and (d) imaginary parts of the energy spectrum, as well as the fractal dimension of in the topologically nontrivial region ($\mu = 0.5$). (e) The minimum values of $|E|$ under OBC and (f) the energy band gap under PBC in the μ–γ plane. The white dashed box represents the phase boundary. The rest parameters are set as $t = 1$, $\Delta = 0.8$, $\eta = 0$, and $N = 100$.

3.3. The nonreciprocal Kitaev model with only nonreciprocal pairing strength

In this section, we present the numerical results for the nonreciprocal Kitaev chain with only nonreciprocal pairing strength, as illustrated in figure 4. In figures 4(a)–(d), we exhibit the real and imaginary parts of the energy spectrum and the fractal dimension Γ as a function of the nonreciprocal pairing strength γ in two different topological phases. In the topologically trivial regime ($\mu = 2.5$), we observe two exceptional points at $\gamma = \pm\sqrt{2.205}$, as depicted in figures 4(a) and (b). While in the topologically nontrivial regime ($\mu = 0.5$), we find two exceptional points at $\gamma = \pm\sqrt{2.81}/2$, as shown in figures 4(c) and (d). Interestingly, we note that the appearance of the exceptional points is independent of the topological phase, and is solely determined by the dispersion relation of equation (12). Moreover, we observe that the system does not exhibit the non-Hermitian skin effect due to fractal dimension of the bulk state $\Gamma \to 1$, which can be explained by the symmetries and Majorana picture without considering it temporarily. We plot the minimum absolute eigenvalues of the energy spectrum under OBC in the μ–γ plane in figure 4(e) and show that the system supports stable degenerate Majorana zero energy modes within the white dashed box when $|\gamma| \leqslant \sqrt{\Delta^2 + \mu^2/4}$ and $|\mu| \leqslant 2$. Furthermore, as depicted in figure 4(f), we present the energy band gap under PBC in the μ–γ plane, which shows the topological phase transitions occurring at $\mu = \pm 2$ and $\gamma = \pm\sqrt{\Delta^2 + \mu^2/4}$ due to the fact that the energy band gap marked by white dashed box undergoes a opening–closing–reopening process. Therefore, we conclude that the nonreciprocal pairing strength γ can induce a topological phase transition, and despite the non-Hermitian nature of the current system, it does not exhibit the non-Hermitian skin effect.

In addition, we calculate the real and imaginary parts of the energy spectrum in the momentum space, as shown in figures 5(a) and (b). It is worth noting that the energy spectrum in the present system is purely real or imaginary, owing to presence of the pseudo-Hermitian symmetries. Specifically, we find that the purely real energy spectrum occurs either at $k = m\pi$ or when $|\gamma| \leqslant \sqrt{\Delta^2 + \mu^2/4}$, and the purely imaginary energy spectrum otherwise. To understand the results more intuitively, we illustrate the schematic diagram in the Majorana basis, as depicted in figure 5(c). Here, the next-nearest-neighbor hopping amplitudes between one type of Majorana fermions b are represented by gray solid lines with γ, while those between the other type of

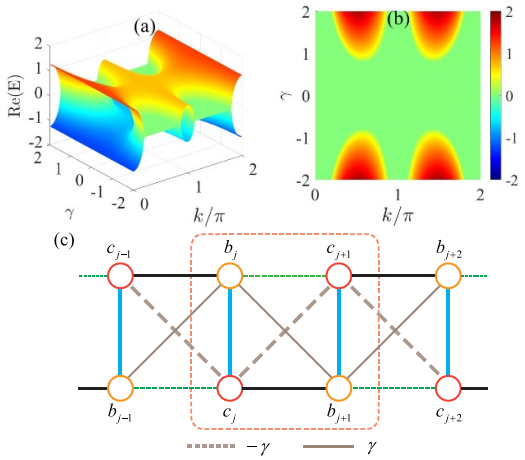

Figure 5. (a) The real part of the energy spectrum as a function of k and γ when $\eta = 0$ and $\mu = 0.5$ in the momentum space. (b) The imaginary part of the energy spectrum in the k–γ plane. (c) The schematic diagram of the nonreciprocal Kitaev model with only the nearest-neighbor nonreciprocal pairing strength in the Majorana basis. The next-nearest-neighbor hopping amplitudes between the same types of Majorana fermions b (c) are γ ($-\gamma$), which are marked by gray solid (dashed) lines. The red dotted box represents a unit cell.

Majorana fermions c are denoted by gray dashed lines with $-\gamma$. We consider a unit cell consisting of four Majorana fermions, which is highlighted by the red dotted box. This configuration leads to zero magnetic flux in the panel, similar to a $\mathcal{PT}$-symmetric system, indicating that the present system is balanced and does not exhibit non-Hermitian skin effect.

4. Topological invariant

In this section, we focus on studying the nonreciprocal Kitaev chain with only the nonreciprocal nearest-neighbor pairing strength, and its corresponding Hamiltonian is given by

$$\mathcal{H}_\gamma(k) = h_x\sigma_x + h_y\sigma_y + h_z\sigma_z. \tag{18}$$

The above equation satisfies TRS, PHS, and CS. Moreover, equation (18) also has the pseudo-Hermitian symmetry, defined as $\xi = \sigma_x\mathcal{T}$, which satisfies

$$\xi\,\mathcal{H}^\dagger{}_\gamma(k)\,\xi^{-1} = \mathcal{H}_\gamma(k), \tag{19}$$

and possesses the following Hermitian counterpart

$$\bar{\mathcal{H}}_\gamma(k) = \bar{h}_y\sigma_y + \bar{h}_z\sigma_z, \tag{20}$$

where $\bar{h}_y = 2\sqrt{\Delta^2 - \gamma^2}\sin k$ and $\bar{h}_z = h_z$. It is convenient for computing the energy spectrum and topological invariant, we can convert it into an off-diagonal matrix form as

$$\tilde{\mathcal{H}}_\gamma(k) = \tilde{h}_x\sigma_x + \tilde{h}_y\sigma_y, \tag{21}$$

by performing the unitary transformation

$$\tilde{\mathcal{H}}_\gamma(k) = U\bar{\mathcal{H}}_\gamma(k)\,U^{-1}, \tag{22}$$

with $\tilde{h}_x = -\bar{h}_z$, $\tilde{h}_y = \bar{h}_y$, and U is a unitary operator

$$U = \frac{1}{\sqrt{2}}\begin{pmatrix} 1 & 1 \\ -1 & 1 \end{pmatrix}. \tag{23}$$

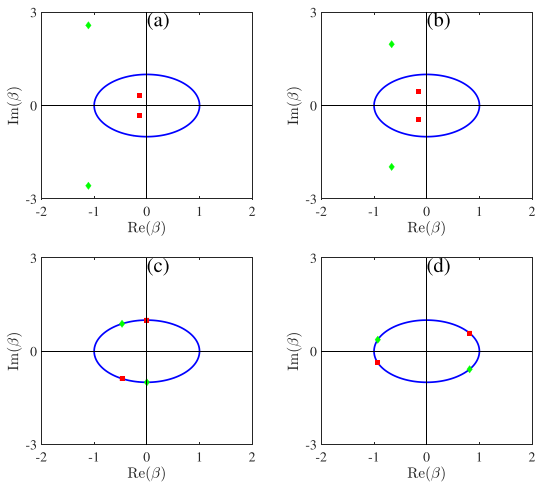

Figure 6. The GBZ marked by blue solid line and the eigenvalues of $R_{\pm}(\beta)$ labeled by red square and green diamond in different parameter regimes. (a) $\gamma = 0.2$, (b) $\gamma = 0.5$, (c) $\gamma = \sqrt{2.81}/2$, (d) $\gamma = 2$. The rest parameters are set as $t = 1$, $\Delta = 0.8$, $\mu = 0.5$, and $\eta = 0$.

Now we define $\beta = e^{ik}$, the non-Bloch Hamiltonian is derived as

$$\tilde{\mathcal{H}}_{\gamma}(\beta) = R_{+}(\beta)\sigma_{+} + R_{-}(\beta)\sigma_{-}, \tag{24}$$

where $R_{\pm}(\beta) = -\mu - (t \pm \sqrt{\Delta^2 - \gamma^2})\beta - (t \mp \sqrt{\Delta^2 - \gamma^2})\beta^{-1}$ and $\sigma_{\pm} = (\sigma_x \pm \sigma_y)/2$. Here, β plays the role of a momentum-like variable, but unlike conventional Bloch theory, it is not restricted to the Brillouin zone. In the non-Hermitian systems, the non-Bloch band theory and the generalized Brillouin zone (GBZ) are used to describe the topological properties of the systems. GBZ can be constructed by $|\beta_2(E)| = |\beta_3(E)|$ for given E in the system, then the continuum bands can be calculated. The winding number [19, 38, 40, 46, 49] can be written as

$$w = \frac{1}{2\pi i}\oint_{l} \mathrm{d}\beta \partial_{\beta} \mathrm{In}\ \det\left(\tilde{\mathcal{H}}_{\gamma}(\beta) - E_{\mathrm{b}}\right), \tag{25}$$

where l and E_{b} are any closed loop and reference base energy independent of the energy spectrum of the system, respectively. The simplified expression of w can be described by

$$w = -\frac{1}{2}\left[N(+) - N(-)\right], N(\pm) = \left[N_{\mathrm{z}}(\pm) - N_{\mathrm{p}}(\pm)\right]_{\mathrm{GBZ}}, \tag{26}$$

where $N_{\mathrm{z}}(\pm)$ and $N_{\mathrm{p}}(\pm)$ represent the number of zero and pole point of $R_{\pm}(\beta)$ inside the GBZ, respectively. It is indeed that number of pole point of $R_{\pm}(\beta)$ is always 1 according to equation (21), i.e. $N_{\mathrm{p}}(\pm) = 1$.

Therefore, the topological invariant of the system can be directly determined by solving the number of zero point of $R_{\pm}(\beta)$, as depicted in figure 6. From figures 6(a) and (b), it is evident that the number of zero point of $R_{+}(\beta)$ is always 2, while of $R_{-}(\beta)$ is 0. Thus, the system belongs to the topologically nontrivial phase characterized by the winding number $w = -1$ in the pseudo-Hermitian symmetry-unbroken region, where purely real energy spectrum and two degenerate Majorana zero energy modes are observed. It indicates the preservation of the bulk-edge correspondence relation. Figure 6(c) illustrates that some eigenvalues of $R_{\pm}(\beta)$ are real and all lie above the GBZ at the critical point. In the pseudo-Hermitian symmetry-broken region, the eigenvalues of $R_{\pm}(\beta)$ are complex and also lie above the GBZ, as shown in figure 6(d).

5. Conclusions

In conclusion, we have investigated the nonreciprocal Kitaev chain along with nearest-neighbor nonreciprocal hopping amplitude and pairing strength from different aspects. For the nonreciprocal Kitaev

chain with only the nonreciprocal hopping amplitude, we observe the non-Hermitian skin effect, the stable existence of degenerate Majorana zero energy modes in topologically nontrivial region, and the absence of a topological phase transition as the nonreciprocity of hopping amplitude increases. Moreover, we also find that the energy spectrum immediately change from real to complex upon the introduction of nonreciprocal hopping amplitude. However, in the presence of nonreciprocal pairing strength, we uncover that the pseudo-Hermitian symmetry is broken during the topological phase transition, and the exceptional points determined by the dispersion relation are independent of the topological phase. Furthermore, we demonstrate the failure of the non-Hermitian skin effect, and calculate the topological invariant to illustrate the bulk-edge correspondence relation in the pseudo-Hermitian symmetry-unbroken region. Our work provides a more comprehensive exploration of the topological properties in the nonreciprocal Kitaev chain and enhances the understanding of the interplay between nonreciprocity and topological phases.

Data availability statement

All data that support the findings of this study are included within the article (and any supplementary files).

Acknowledgment

This work was supported by the National Natural Science Foundation of China under Grant Nos. 12375020, 12074330, 62071412, 2074094, and 62201493.

Appendix

We first analyze whether the energy spectrum in the momentum space is real or complex when neither η nor γ is zero, as shown in figure 7. The closing point of the energy gap satisfies $E(k) = 0$ in equation (12), which means $(\mu + 2t\cos k)^2 + 4(\Delta^2 + \eta^2 - \gamma^2)\sin^2 k = 0$. Specially, the energy spectrum is purely real when $k = 0$ due to $E(k) = \pm\sqrt{(\mu + 2t)^2}$, as shown in figures 7(a) and (b). For the other special cases $k = 0.5\pi$, we have $E(k) = \pm\sqrt{\mu^2 + 4(\Delta^2 - \gamma^2)} - 2i\eta$. From figures 7(c) and (d), the energy spectrum is complex when $|\gamma| < \sqrt{\Delta^2 + \mu^2/4}$, and then becomes purely imaginary when $|\gamma| > \sqrt{\Delta^2 + \mu^2/4}$ and $|\gamma| \neq \sqrt{\eta^2 + \Delta^2 + \mu^2/4}$. However, the energy spectrum is 0 and $-4i\eta$ in the special case of $|\gamma| = \sqrt{\eta^2 + \Delta^2 + \mu^2/4}$, which is multiple degenerate.

Furthermore, we also attempt to provide the phase diagram as a function of η and γ for a trivial μ and nontrivial μ in figure 8. It is seen from figure 8(a) that the topologically nontrivial phase characterized by the zero energy modes always exists when $\gamma < 0.8$ and regardless of the value of η, meaning that a topological phase transition is not induced. Once $\gamma > 0.8$, the system undergoes a phase transition from a coalescing phase to a gapless phase as η increases. For the trivial case $\mu = 2.5$, a phase transition point at $\gamma \approx 1.1$ separates the topologically trivial phase from the gapless phase regardless of the value of η, as shown in figure 8(b).

To provide a clearer visualization of the different phases, we display the real part of the energy spectrum corresponding to the red dashed line in figure 8 as a function of η or γ is shown in figure 9. We can observe that the zero-energy modes persist as η increases when $\gamma = 0.7$ for $\mu = 0.5$, indicating the system remains in the topologically nontrivial phase, as shown in figure 9(a). However, the real part of the energy spectrum is coalescing when $\eta \lesssim 0.5$ and then becomes gapless when $\eta \gtrsim 0.5$ for $\gamma = 1.0$, as shown in figure 9(b). The phase transition point at $\eta \approx 0.5$ is marked by the red dashed line. It can be seen from figures 9(c) and (d) that the system always supports the topologically trivial phase for $\gamma < 1.1$ and the gapless phase for $\gamma > 1.1$ regardless of the value of η. Similarly, the phase transition point at $\gamma \approx 1.1$ is marked by the red dashed line. These results are agreement with the phase diagram in figure 8.

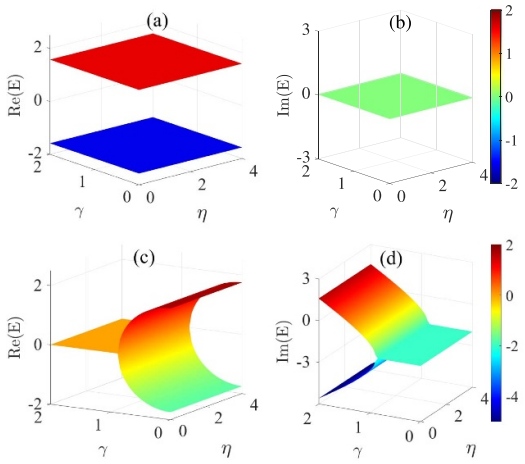

Figure 7. The real and imaginary parts of the energy spectrum as a function of η and γ for different k in the momentum space. (a) and (b) $k=0$. (c) and (d) $k=0.5\pi$. The other parameters are set as $t=1$, $\Delta=0.8$, and $\mu=0.5$.

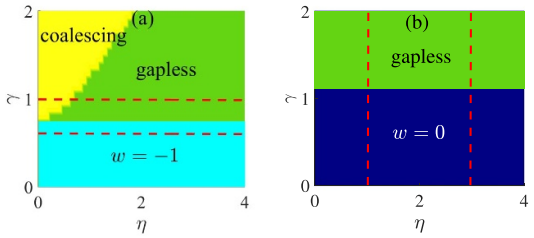

Figure 8. The phase diagram as a function of η and γ for different μ. (a) $\mu=0.5$. (b) $\mu=2.5$. The other parameters are set as $t=1$, and $\Delta=0.8$.

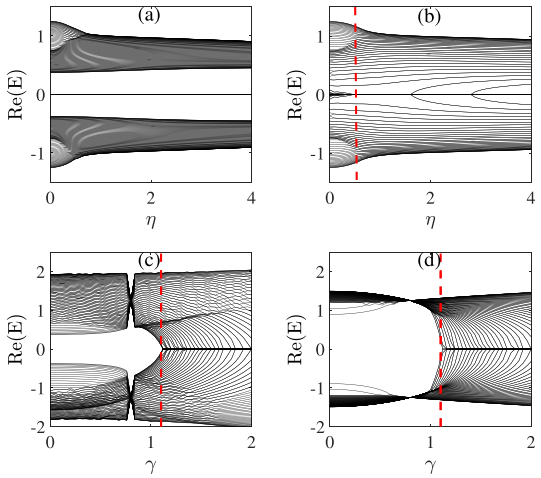

Figure 9. The real part of the energy spectrum as a function of η or γ. (a) $\mu=0.5$ and $\gamma=0.7$. (b) $\mu=0.5$ and $\gamma=1.0$. (c) $\mu=2.5$ and $\eta=1.0$. (d) $\mu=2.5$ and $\eta=3.0$. The other parameters are set as $t=1$, $\Delta=0.8$, and $N=100$.

ORCID iDs

Wen-Xue Cui https://orcid.org/0000-0001-8248-8158
Shutian Liu https://orcid.org/0000-0001-9748-0175
Hong-Fu Wang https://orcid.org/0000-0002-6778-6330

References

[1] Kitaev A Y 2001 Unpaired Majorana fermions in quantum wires *Phys. Usp.* **44** 131
[2] Stern A 2010 Non-Abelian states of matter *Nature* **464** 187
[3] Nayak C, Simon S H, Stern A, Freedman M and Das Sarma S 2008 Non-Abelian anyons and topological quantum computation *Rev. Mod. Phys.* **80** 1083
[4] Alicea J 2012 New directions in the pursuit of Majorana fermions in solid state systems *Rep. Prog. Phys.* **75** 076501
[5] Qi L, Yan Y, Wang G L, Zhang S and Wang H F 2019 Bosonic Kitaev phase in a frequency-modulated optomechanical array *Phys. Rev.* A **100** 062323
[6] Yokomizo K and Murakami S 2021 Non-Bloch band theory in bosonic Bogoliubov-de Gennes systems *Phys. Rev.* B **103** 165123
[7] Wakatsuki R, Ezawa M and Nagaosa N 2014 Majorana fermions and multiple topological phase transition in Kitaev ladder topological superconductors *Phys. Rev.* B **89** 174514
[8] Yan Y, Qi L, Wang D Y, Xing Y, Wang H F and Zhang S 2020 Topological phase transition and phase diagrams in a two-leg Kitaev ladder system *Ann. Phys.* **532** 1900479
[9] Read N and Green D 2000 Paired states of fermions in two dimensions with breaking of parity and time-reversal symmetries and the fractional quantum Hall effect *Phys. Rev.* B **61** 10267
[10] Ivanov D A 2001 Non-Abelian statistics of half-quantum vortices in p-wave superconductors *Phys. Rev. Lett.* **86** 268
[11] Das Sarma S, Nayak C and Tewari S 2006 Proposal to stabilize and detect half-quantum vortices in strontium ruthenate thin films: non-Abelian braiding statistics of vortices in a $p_x + ip_y$ superconductor *Phys. Rev.* B **73** 220502(R)
[12] Fu L and Kane C L 2008 Superconducting proximity effect and Majorana fermions at the surface of a topological insulator *Phys. Rev. Lett.* **100** 096407
[13] Mourik V, Zuo K, Frolov S M, Plissard S R, Bakkers E P A M and Kouwenhoven L P 2012 Signatures of Majorana fermions in hybrid superconductor-semiconductor nanowire devices *Science* **336** 1003
[14] Deng M T, Yu C L, Huang G Y, Larsson M, Caroff P and Xu H Q 2012 Anomalous zero-bias conductance peak in a Nb-InSb nanowire-Nb hybrid device *Nano Lett.* **12** 6414
[15] Rokhinson L P, Liu X and Furdyna J K 2012 The fractional a.c. Josephson effect in a semiconductor-superconductor nanowire as a signature of Majorana particles *Nat. Phys.* **8** 795
[16] Nadjperge S, Drozdov I K, Li J, Chen H, Jeon S, Seo J, MacDonald A H, Bernevig B A and Yazdani A 2014 Observation of Majorana fermions in ferromagnetic atomic chains on a superconductor *Science* **346** 602
[17] Mebrahtu H T, Borzenets I V, Zheng H, Bomze Y V, Smirnov A I, Florens S, Baranger H U and Finkelstein G 2013 Observation of Majorana quantum critical behaviour in a resonant level coupled to a dissipative environment *Nat. Phys.* **9** 732
[18] Lee E J H, Jiang X, Houzet M, Aguado R, Lieber C M and Franceschi S D 2014 Spin-resolved Andreev levels and parity crossings in hybrid superconductor-semiconductor nanostructures *Nat. Nanotechnol.* **9** 79
[19] Ashida Y, Gong Z and Ueda M 2020 Non-Hermitian physics *Adv. Phys.* **69** 249
[20] Rotter I and Bird J P 2015 A review of progress in the physics of open quantum systems: theory and experiment *Rep. Prog. Phys.* **78** 114001
[21] Cao J, Yi X X and Wang H F 2020 Band structure and the exceptional ring in a two-dimensional superconducting circuit lattice *Phys. Rev.* A **102** 032619
[22] Mostafazadeh A 2002 Pseudo-Hermiticity versus $\mathcal{PT}$ symmetry: the necessary condition for the reality of the spectrum of a non-Hermitian Hamiltonian *J. Math. Phys.* **43** 205
[23] Mostafazadeh A 2002 Pseudo-Hermiticity versus $\mathcal{PT}$-symmetry. II. A complete characterization of non-Hermitian Hamiltonians with a real spectrum *J. Math. Phys.* **43** 2814
[24] Mostafazadeh A 2003 Pseudo-Hermiticity and generalized $\mathcal{PT}$- and CPT-symmetries *J. Math. Phys.* **44** 974
[25] Zhao X, Xing Y, Qi L, Liu S, Zhang S and Wang H F 2021 Real-potential-driven anti-$\mathcal{PT}$-symmetry breaking in non-Hermitian Su-Schrieffer-Heeger model *New. J. Phys.* **23** 073043
[26] Xing Y, Qi L, Cao J, Wang D Y, Bai C H, Wang H F, Zhu A D and Zhang S 2017 Spontaneous PT-symmetry breaking in non-Hermitian coupled-cavity array *Phys. Rev.* A **96** 043810
[27] Hatano N and Nelson D R 1996 Localization transitions in non-Hermitian quantum mechanics *Phys. Rev. Lett.* **77** 570
[28] Ghatak A and Das T 2019 New topological invariants in non-Hermitian systems *J. Phys.: Condens. Matter* **31** 263001
[29] Shen H, Zhen B and Fu L 2018 Topological band theory for non-Hermitian Hamiltonians *Phys. Rev. Lett.* **120** 146402
[30] Jiang H, Yang C and Chen S 2018 Topological invariants and phase diagrams for one-dimensional two-band non-Hermitian systems without chiral symmetry *Phys. Rev.* A **98** 052116
[31] Kunst F K and Dwivedi V 2019 Non-Hermitian systems and topology: a transfer-matrix perspective *Phys. Rev.* B **99** 245116
[32] Leykam D, Bliokh K Y, Huang C, Chong Y D, Nori F and Modes E 2017 Degeneracies and topological numbers in non-Hermitian systems *Phys. Rev. Lett.* **118** 040401
[33] Lee T E 2016 Anomalous edge state in a non-Hermitian lattice *Phys. Rev. Lett.* **116** 133903
[34] Kawabata K, Shiozaki K and Ueda M 2018 Anomalous helical edge states in a non-Hermitian Chern insulator *Phys. Rev.* B **98** 165148
[35] Wang X R, Guo C X and Kou S P 2020 Defective edge states and number-anomalous bulk-boundary correspondence in non-Hermitian topological systems *Phys. Rev.* B **101** 121116(R)
[36] Bergholtz E J, Budich J C and Kunst F K 2021 Exceptional topology of non-Hermitian systems *Rev. Mod. Phys.* **93** 015005
[37] Yin C, Jiang H, Li L, Lü R and Chen S 2018 Geometrical meaning of winding number and its characterization of topological phases in one-dimensional chiral non-Hermitian systems *Phys. Rev.* A **97** 052115
[38] Kawabata K, Shiozaki K, Ueda M and Sato M 2019 Symmetry and topology in non-Hermitian physics *Phys. Rev.* X **9** 041015
[39] Kawabata K, Higashikawa S, Gong Z, Ashida Y and Ueda M 2019 Topological unification of time-reversal and particle-hole symmetries in non-Hermitian physics *Nat. Commun.* **10** 297
[40] Zhou H and Lee J Y 2019 Periodic table for topological bands with non-Hermitian symmetries *Phys. Rev.* B **99** 235112
[41] Lin S, Jin L and Song Z 2019 Symmetry protected topological phases characterized by isolated exceptional points *Phys. Rev.* B **99** 165148
[42] Rudner M S and Levitov L S 2009 Topological transition in a non-Hermitian quantum walk *Phys. Rev. Lett.* **102** 065703
[43] Esaki K, Sato M, Hasebe K and Kohmoto M 2011 Edge states and topological phases in non-Hermitian systems *Phys. Rev.* B **84** 205128

[44] Hu Y C and Hughes T L 2011 Absence of topological insulator phases in non-Hermitian $\mathcal{PT}$-symmetric Hamiltonians *Phys. Rev.* B **84** 153101
[45] Lieu S 2018 Topological phases in the non-Hermitian Su-Schrieffer-Heeger model *Phys. Rev.* B **97** 045106
[46] Gong Z, Ashida Y, Kawabata K, Takasan K, Higashikawa S and Ueda M 2018 Topological phases of non-Hermitian systems *Phys. Rev.* X **8** 031079
[47] Liu C H, Jiang H and Chen S 2019 Topological classification of non-Hermitian systems with reflection symmetry *Phys. Rev.* B **99** 125103
[48] Zhang K L, Wu H C, Jin L and Song Z 2019 Topological phase transition independent of system non-Hermiticity *Phys. Rev.* B **100** 045141
[49] Yao S and Wang Z 2018 Edge states and topological invariants of non-Hermitian systems *Phys. Rev. Lett.* **121** 086803
[50] Yao S, Song F and Wang Z 2018 Non-Hermitian Chern bands *Phys. Rev. Lett.* **121** 136802
[51] Qi L, He A L, Wang H F and Liu Y 2023 Topological semimetal phase and dynamical characterizationin a non-Hermitian two-leg ladder model *Phys. Rev.* B **107** 115107
[52] Deng T S and Yi W 2019 Non-Bloch topological invariants in a non-Hermitian domain wall system *Phys. Rev.* B **100** 035102
[53] Song F, Yao S and Wang Z 2019 Non-Hermitian skin effect and chiral damping in open quantum systems *Phys. Rev. Lett.* **123** 170401
[54] Longhi S 2019 Probing non-Hermitian skin effect and non-Bloch phase transitions *Phys. Rev. Res.* **1** 023013
[55] Lee C H and Thomale R 2019 Anatomy of skin modes and topology in non-Hermitian systems *Phys. Rev.* B **99** 201103(R)
[56] Xiong Y 2018 Why does bulk boundary correspondence fail in some non-Hermitian topological models *J. Phys. Commun.* **2** 035043
[57] Kunst F K, Edvardsson E, Budich J C and Bergholtz E J 2018 Biorthogonal bulk-boundary correspondence in non-Hermitian systems *Phys. Rev. Lett.* **121** 026808
[58] Herviou L, Bardarson J H and Regnault N 2019 Defining a bulk-edge correspondence for non-Hermitian Hamiltonians via singular-value decomposition *Phys. Rev.* A **99** 052118
[59] Yokomizo K and Murakami S 2019 Non-Bloch band theory of non-Hermitian systems *Phys. Rev. Lett.* **123** 066404
[60] Imura K I and Takane Y 2019 Generalized bulk-edge correspondence for non-Hermitian topological systems *Phys. Rev.* B **100** 165430
[61] Liu X J, Wong C L M and Law K T 2014 Non-Abelian Majorana doublets in time-reversal-invariant topological superconductors *Phys. Rev.* X **4** 021018
[62] Yuce C 2016 Majorana edge modes with gain and loss *Phys. Rev.* A **93** 062130
[63] Menke H and Hirschmann M M 2017 Topological quantum wires with balanced gain and loss *Phys. Rev.* B **95** 174506
[64] Zeng Q B, Zhu B, Chen S, You L and Lü R 2016 Non-Hermitian Kitaev chain with complex on-site potentials *Phys. Rev.* A **94** 022119
[65] Klett M, Cartarius H, Dast D, Main J and Wunner G 2017 Relation between $\mathcal{PT}$-symmetry breaking and topologically nontrivial phases in the Su-Schrieffer-Heeger and Kitaev models *Phys. Rev.* A **95** 053626
[66] Wang X, Liu T, Xiong Y and Tong P 2015 Spontaneous $\mathcal{PT}$-symmetry breaking in non-Hermitian Kitaev and extended Kitaev models *Phys. Rev.* A **92** 012116
[67] Li C, Zhang X Z, Zhang G and Song Z 2018 Topological phases in a Kitaev chain with imbalanced pairing *Phys. Rev.* B **97** 115436
[68] Zhao X M, Guo C X, Kou S P, Zhuang L and Liu W M 2021 Defective Majorana zero modes in a non-Hermitian Kitaev chain *Phys. Rev.* B **104** 205131
[69] der Pino J, Slim J J and Verhagen E 2022 Non-Hermitian chiral phononics through optomechanically induced squeezing *Nature* **606** 82
[70] Xu X W, Xu Y, Li B, Jing H and Chen A X 2020 Nonreciprocity via nonlinearity and synthetic magnetism *Phys. Rev. Appl.* **13** 044070
[71] Heeger A J, Kivelson S, Schrieffer J R and Su W P 1988 Solitons in conducting polymers *Rev. Mod. Phys.* **60** 781
[72] Qi L, Wang G L, Liu S T, Zhang S and Wang H F 2020 Engineering the topological state transfer and topological beam splitter in an even-sized Su-Schrieffer-Heeger chain *Phys. Rev.* A **102** 022404
[73] Xiu T, Cheng S, Guo H and Gao X 2021 Fate of Majorana zero modes, exact location of critical states and unconventional real-complex transition in non-Hermitian quasiperiodic lattices *Phys. Rev.* B **103** 104203
[74] Cai X 2021 Localization and topological phase transitions in non-Hermitian Aubry-André-Harper models with *p*-wave pairing *Phys. Rev.* B **103** 214202
[75] Wang Y, Xia X, Zhang L, Yao H, Chen S, You J, Zhou Q and Liu X J 2020 One-dimensional quasiperiodic mosaic lattice with exact mobility edges *Phys. Rev. Lett.* **125** 196604